

Learning Domain Invariant Representations for Generalizable Person Re-Identification

Yi-Fan Zhang, Zhang Zhang, Da Li, Zhen Jia,
Liang Wang, *Fellow, IEEE* and Tieniu Tan, *Fellow, IEEE*

Abstract—Generalizable person Re-Identification (ReID) aims at learning ready-to-use cross-domain representations for direct cross-data evaluation, which has attracted growing attention in the recent computer vision (CV) community. In this work, we construct a structural causal model (SCM) among identity labels, identity-specific factors (clothing/shoes color *etc.*), and domain-specific factors (background, viewpoints *etc.*). According to the causal analysis, we propose a novel Domain Invariant Representation Learning for generalizable person Re-Identification (DIR-ReID) framework. Specifically, we propose to disentangle the identity-specific and domain-specific factors into two independent feature spaces, based on which an effective backdoor adjustment approximate implementation is proposed for serving as a causal intervention towards the SCM. Extensive experiments have been conducted, showing that DIR-ReID outperforms state-of-the-art (SOTA) methods on large-scale domain generalization (DG) ReID benchmarks.

Index Terms—Generalizable person Re-Identification, disentanglement, backdoor adjustment.

I. INTRODUCTION

Person Re-Identification (ReID) [1] aims at matching person images of the same identity across multiple camera views. In previous work, most ReID models are trained and tested on the same dataset, termed fully-supervised methods [2], [3], or adapted by unlabeled data in target domains different from the training datasets, termed unsupervised domain adaptation (UDA) methods [4], [5]. Although recent fully-supervised methods have achieved remarkable performance, they tend to fail catastrophically when tested in out-of-distribution (OOD) settings. Fig. 1 illustrates the fragility of two representative fully-supervised models, *i.e.*, the DG-Net [3] and ISGAN [6], which both get very high rank-1 accuracies when model training and test are performed on the same Market1501 dataset [7]. However, the rank-1 accuracies drop to 18.7% and 27.8% respectively when directly tested on the GRID

Yi-Fan Zhang, Zhang Zhang, Da Li, and Zhen Jia are with the National Laboratory of Pattern Recognition (NLPR), Center for Research on Intelligent Perception and Computing (CRIPAC), Institute of Automation, Chinese Academy of Sciences (CASIA), Beijing 100190, China, and also with the School of Artificial Intelligence, University of Chinese Academy of Sciences (UCAS), Beijing 100049, China (e-mail: yifanzhang.cs@gmail.com; zzhang@nlpr.ia.ac.cn, da.li@cripac.ia.ac.cn, zhen.jia@nlpr.ia.ac.cn).

Liang Wang and Tieniu Tan are with the National Laboratory of Pattern Recognition, Center for Research on Intelligent Perception and Computing, Institute of Automation, Chinese Academy of Sciences (CASIA), Beijing 100190, China, also with the University of Chinese Academy of Sciences, Beijing 100044, China, and also with the Center for Excellence in Brain Science and Intelligence Technology, Institute of Automation, Chinese Academy of Sciences (CASIA), Beijing 100190, China (e-mail: wangliang@nlpr.ia.ac.cn; tni@nlpr.ia.ac.cn)

Corresponding author: Zhang Zhang.

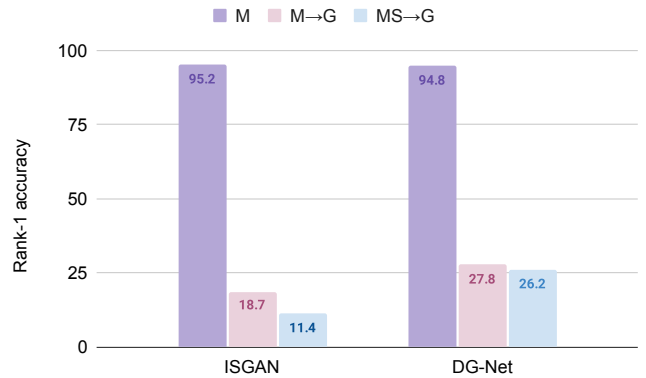


Fig. 1. Performance of two representative models. M: Train and test on Market1501. M→G: Trained on Market1501 and tested on GRID. MS→G: Trained on multi-source datasets and tested on GRID.

dataset [8], suggesting the weak extrapolation capability and poor robustness of fully supervised methods. We further train these two models over multiple source domains (the details of sources are in Section IV-A). However, *the even worse performance are obtained*, which indicates the challenge of ReID in the OOD settings. To tackle these problems, a number of UDA methods have been proposed to mitigate the domain gap without the need for extensive manual annotations in new target domains. However, they still need to collect large amounts of unlabeled data for UDA retraining. These problems severely hinder real-world applications of current person ReID techniques.

To tackle the above challenges, we focus on a more realistic and practical setting: generalizable person ReID, where the model is trained on multiple large-scale public datasets and on unseen domains directly without any model adaptations. The generalizable person ReID is originally formulated as a problem of domain generalization (DG) [9], which is more practicable than the traditional ReID paradigm since the ready-to-use models can work on any new settings without the requirement of data collection, annotation, and model updating.

Assuming that a person image can be factorized into two latent factors, *i.e.*, the identity-specific factors S (*e.g.*, appearances, body shapes) and the domain-specific factors V (*e.g.*, imaging conditions such as backgrounds, viewing angles, illuminations *etc.*), we first present a structural causal model (SCM) for generalizable person ReID, which provides insights for the poor generalization of traditional ReID models when

applied to unseen domains. Here, we highlight the potential reason for poor generalization ability: the domain-specific factors V confound the identity-specific factors S as well as the identity label Y , so that the spurious correlations between V and S hinder the model from making a robust prediction on identity label Y based on S . Thus, a novel domain-invariant representation learning paradigm is proposed for generalizable person ReID, termed DIR-ReID, which disentangles the two latent factors V and S to remove spurious features.

Specially, a Multi-Domain Disentangled Adversarial Neural Network (MDDAN) is first proposed to jointly learn two encoders for embedding identity-specific and domain-specific factors from multiple public ReID datasets, where the adversarial learning principle is adopted to exclude the domain-related information from the embedded identity specific representations. Then a differentiable backdoor adjustment block (BA) is proposed to approximate the interventional distribution [10], which can pursue the true causality between identity-specific factors and identity labels. These two components (MDDAN and BA) are integrated as an end-to-end learning framework for generalizable person ReID, namely DIR-ReID.

To sum up, the contributions of our work can be summarized as follows:

- For the first time, a causal perspective on the analysis of generalizable person ReID is introduced, by which the domain-specific factor is essentially a confounder that causes spurious correlations between person features and identity labels in new target domains.
- Thanks to the above analysis, a novel domain-invariant representation learning framework is proposed for generalizable person ReID, namely DIR-ReID, where an MDDAN block is adopted to disentangle identity-specific and domain-specific factors from multiple data sources. Then a BA block is adopted to approximate causal interventions. Mathematical analysis proves the characteristics of our method;
- Comprehensive experiments are conducted to demonstrate the effectiveness of the proposed DIR-ReID model. Our method achieves superior performance in comparison with state-of-the-art (SOTA) methods on large-scale generalizable person ReID benchmarks.

II. RELATED WORK

Single-domain Person ReID Existing works of single-domain person ReID (*i.e.*, supervised person ReID) usually depend on the assumption that training and testing data are independent and identically distributed. They usually design to learn discriminative features [11] or develop efficient metrics [12]. With the rapid development of deep Convolutional Neural Networks (CNNs), single-domain person ReID has achieved great progress. Some of the CNN-based methods introduce human parts [13], [14], poses [15], and masks [16] to improve the robustness of extracted features. [17] propose a multi-level Context-aware Part Attention(CPA) model to learn discriminative and robust local part features. [18] propose a Homogeneous Augmented Tri-Modal (HAT) learning method for visible modality and night-time infrared modality. [19] introduces an online co-refining (CORE) framework

with dynamic mutual learning. [20] designs an intra-modality weighted-part attention (IWPA) to construct part-aggregated representation. And some other methods use deep metric learning to learn appropriate similarity measures [21]. Due to the space limitation, many important works cannot be covered. A well-summarized survey on person reID can be found at [1]. Despite the encouraging performance under the single-domain setup, current fully-supervised ReID models degrade significantly when deployed to an unseen domain.

Cross-domain Person ReID Unsupervised Domain Adaptation (UDA) technologies have great progress [22] and been widely adopted for cross-domain person ReID. The UDA-based ReID methods usually attempt to transfer the knowledge learned from the labeled source domains to target domains one depending on target-domain images [4], [23], features [24] or metrics [25]. Another group of UDA-based methods [26], [27] propose to explore hard or soft pseudo labels in the unlabeled target domain using its data distribution geometry. Though UDA-based methods improve the performance of cross-domain ReID to a certain extent, most of them require a large amount of unlabeled target data for model retraining.

Generalizable Person ReID Recently, generalizable person ReID methods [9] are proposed to learn a model that can generalize to unseen domains without the requirement of model adaptation and data collection in target domains. Existing methods mainly follow a meta-learning pipeline or utilize domain-specific heuristics. Jia *et al.*[28] learn the domain-invariant features by integrating Instance Normalization (IN) into the network to filter out style factors. Jin *et al.*[29] extend the work [28] by restituting the identity-relevant information to network to ensure the model discrimination. Lin *et al.*[30] propose a feature generalization mechanism by integrating the adversarial auto-encoder and Maximum Mean Discrepancy (MMD) alignment. Song *et al.*[9] propose a Domain-Invariant Mapping Network (DIMN) following the meta-learning pipeline. There also have some studies for learning domain-invariant features, *e.g.*, DANN [31], DDAN [32] and CaNE [33]. The difference between DIR-ReID and these methods is detailed in Section III-F.

Domain Generalization In the machine learning community, domain/OOD generalization [34], [35], [36], [37] aims to learn representations $\Phi(X)$ that is invariant across environments \mathcal{E} so that model can well extrapolate in unseen environments. The problem can be formulated as $\min_{\Phi} \max_{e \in \mathcal{E}} \mathbb{E}[l(y, \Phi(x)) \mid E = e]$. Representative approaches such as IRM [38] have been proposed to address this challenge. However, the IRM would fail catastrophically unless the test data are sufficiently similar to the training distribution [39]. To alleviate these challenges, we adopt a causal representation [40] framework termed DIR-ReID, to explicitly remove the confounding effects of spurious features via backdoor adjustment.

Causality for CV Causal Representation Learning [40] combines machine learning and causal inference and has attracted increasing attention within a learning paradigm to improve generalization and trustworthiness. Simultaneously, there is a growing number of CV tasks that benefit from causality [41], [42], [43]. Most of them focus on measuring

causal effects: disentangling the desired model effects [44], and modularizing reusable features that generalize well [45]. Recently, causal intervention is also introduced into some CV researches [46], [47], [48]. Specifically, CONTA [49] removes the confounding bias in image-level classification by backdoor adjustment and thus provides better pseudo-masks as ground truth for optimizing the subsequent segmentation model. IFSL [50] believes that pre-training is a confounding factor that hurts the performance of few-shot learning (FSL). Thus, they propose an SCM in the FSL process and then develop three practical implementations based on the backdoor adjustment. We also adopt the SCM [51] to model causal effects in generalizable person ReID, where the causal analysis clearly provides the explanations why traditional methods work poorly in unseen domains and then guides the design of the proposed DIR-ReID framework.

III. LEARNING DISENTANGLED AND INVARIANT REPRESENTATIONS

In this section, we first introduce the proposed SCM to analyze spurious correlations between domain-specific factors V and identity labels Y . Then, a DIR-ReID framework is proposed to learn domain-invariant features for generalizable person ReID, where a BA block approximates the interventional distribution to capture the true causality between identity-specific factors S and identity labels Y . Finally, a theoretical analysis is taken for a better understanding of our method.

A. SCM for Generalizable Person ReID

year=2022 Inspired by current research on harnessing causality in machine learning [41], we propose an SCM to analyze disentanglement and generalization in person ReID models.

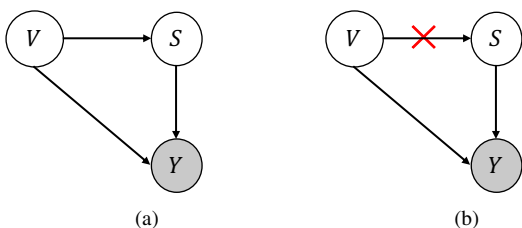


Fig. 2. Graphical representation of person ReID methods. S, V : identity-specific and domain-specific factors, Y : identity labels. Gray circles denote observable variables. (a) Traditional ReID model where $P(Y|S) \neq P(Y|do(S))$. (b) Interventional ReID model where $P(Y|S) \approx P(Y|do(S))$.

Following the causal models in [52], [53], we use the SCM (in Fig. 2(a)) to describe the causal relationships between person images and person identities, where Y denotes the observable variables of identity labels, S and V are the latent variables indicating identity-specific and domain-specific factors, respectively. As shown in the model, there are three kinds of causal relationships as follows.

$S \rightarrow Y$. Identity-specific factors S directly cause Y , which means that person identities are mainly determined by their

identity-specific information, such as clothing styles, body shapes, *etc.*

$V \rightarrow S, V \rightarrow Y$. In real scenarios, there are also some confounders $v_i \in V$ (*e.g.*, backgrounds, illuminations and view-points) that affect both identity factors S and person identities Y . The $V \rightarrow S$ edge indicates the spurious correlations between S and V in the real world. $V \rightarrow Y$ denotes the influences of contextual environments in V on Y . For example, most pedestrians in CUHK03 dataset are captured by high-definition cameras on the campus. Although for some early ReID datasets, *e.g.*, GRID [8] and PRID [54], the low resolution, varying illumination conditions, and various parameters of imaging devices (domain-specific factors) make the appearance of persons vary greatly, even for the same color clothes. For example, the pedestrians in column 1 of Fig. 3 are all wearing white, however, their appearance, such as clothing colors (identity-specific factors) will be influenced by some confounders in the domain-specific factors¹. Thus, there are spurious correlations between S and V and V also confounds the prediction of identity labels Y .

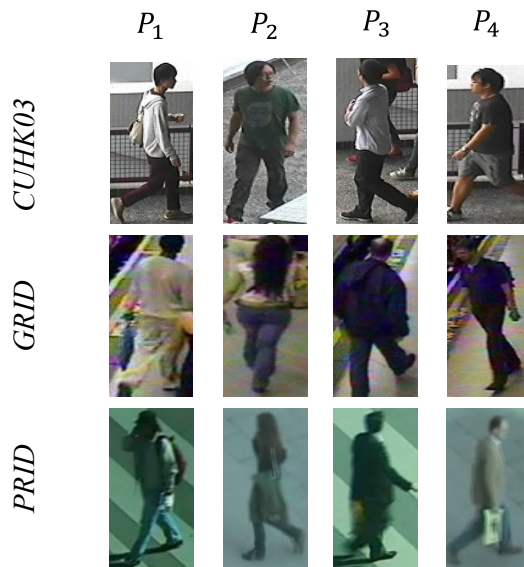


Fig. 3. Spurious correlations between domain-specific factors and identity-specific factors.

An ideal ReID model should capture the true causality between S and Y , which can be generalized to other unseen domains. However, from the SCM in Fig. 2(a), the conventional correlation $P(Y|S)$ fails to do so, because the likelihood of Y given S is not only influenced by “ S causes Y ” via $S \rightarrow Y$, but also spurious correlations via $V \rightarrow Y$. Therefore, to pursue the true causality between S and Y , we need to adopt the causal intervention [10] $P(Y|do(S))$ instead of the likelihood $P(Y|S)$ for the ReID model.

¹The white cloth of P_1 in GRID is more yellowish and that of P_1 in PRID is more greenish

B. Preliminaries of Causal Intervention

The causal intervention seeks the true causal effect of one variable on another, and it is appealing for the objective of DG ReID: given one pedestrian image x_i , we hope the model prediction (pedestrian entity) is faithful only to the semantic feature S , while removing the effects of spurious associations from domain-specific factors V . We use Fig. 2 for example, where domain-specific factors V (e.g., imaging conditions such as backgrounds, viewing angles, illuminations *etc.*) affect both S and Y , leading to spurious correlations if only learning from $P(Y|S)$. To see this, by using the Bayes rule:

$$P(Y|S) = \sum_v P(Y|S, v)P(v|S), \quad (1)$$

where v is an instance in V , which introduces the observational bias. Referring to the analyses in [46], [47], we assume that the training dataset contains much more pedestrian identities from the CUHK03 dataset, where S denotes the semantic information of a pedestrian and $v_{c3} \in V$ the domain-specific factors of the CUHK03 dataset. After training, $P(v_{c3}|S) \approx 1$, hence $P(Y|S)$ degrades to $P(Y|S, v_{c3})$, which the supervised ReID methods actually do. Thus, conventional ReID methods tend to build strong connections between domain-specific factors and pedestrian identities in one domain, where the ReID model is contaminated by the backdoor path $S \leftarrow V \rightarrow Y$.

Do-operation [51] removes certain relationships in the causal graph and replaces a factor with a constant. In our setting, the dependency between V and S should be cut off and the intervention posterior $P(Y|do(S))$ by applying do-operation will be:

$$P(Y|do(S)) = \sum_v P(Y|S, v)P(v). \quad (2)$$

Compared to Eq.(1), the key difference is that the adjustment weight $P(v|S)$ is changed to $P(v)$ because V is no longer dependent on S . After the intervention, the cut-off (Fig. 2(b)). This encourages DG-ReID models to maximize $P(Y|S, v)$ for every style factor v , only subject to a prior $P(v)$.

C. Causal Intervention via Backdoor Adjustment

The above formulation only gives a causal quantity $P(Y|do(S))$ without further *identification* or grounding methods for computing it from purely statistical quantities. Therefore, we propose to use the backdoor adjustment [55] to identify and compute $P(Y|do(S))$ without the need for an ideal dataset². The back-door adjustment assumes that we can stratify the analysis by a number of confounding factors, *i.e.*, $V = \{v_i\}_{i=1}^{|V|}$, where each v_i is the domain-specific factor corresponding to a certain camera view, illumination condition, *etc.*. Formally, the backdoor adjustment for the graph in Fig. 2(b) is (the detailed proof is shown in Appendix A):

²An ideal dataset has images of every pedestrian in all backgrounds and illumination conditions, which is unbiased and has few spurious correlations. Namely, there is no edge $V \rightarrow S$ and then $P(Y|S) = P(Y|do(S))$.

$$P(Y|do(S = s_k)) = \sum_{i=1}^{|V|} P(Y|S = s_k, V = v_i)P(V = v_i) \quad (3)$$

To calculate the above intervention distribution, there are still two challenges: (i) it is hard to instantiate v and s , namely learning two embedding functions, $v_i = f_v(x_i)$ and $s_i = f_s(x_i)$ where x_i is the i -th person image. (ii) it is almost impossible to enumerate all domain-specific factors V . Next, we will offer a practical implementation of Eq.(3): DIR-ReID.

D. The DIR-ReID Framework

Notations and Problem Formulation. For generalized person ReID, we have access to G labeled datasets $\mathcal{D} = \{\mathcal{D}_g\}_{g=1}^G$. Each dataset $\mathcal{D}_g = \{(x_i, y_i, d_i)\}_{i=1}^{N_g}$, where N_g is the number of images in \mathcal{D}_g . The i -th data sample in \mathcal{D}_g can be denoted as a triplet (x_i, y_i, d_i) , where x_i, y_i, d_i denotes the image, identity label and the domain label respectively. In the training phase, we train a DG model using $N = \sum_{g=1}^G N_g$ aggregated image-label pairs from all source domains. In the testing phase, we perform a retrieval task on unseen target domains without additional model updates.

As analyzed in Section III-C, the challenges are (i) how to get the representations of S and V from observation X . (ii) how to approximately marginalize over the domain-specific factors V . Here, we propose DIR-ReID to tackle these challenges. DIR-ReID consists of two blocks, as shown in Fig. 4.

(i) Multi-Domain Disentangled Adversarial Neural Network (MDDAN): MDDAN consists of two sub-blocks: (1) Identity adversarial learning block, which is a domain-agnostic, identity-aware encoder f_S to obtain identity-specific factors. (2) Domain factors learning block, which is a domain-aware encoder f_V to identify domain-specific factors.

(ii) Backdoor adjustment block, which approximates backdoor adjustment in Eq.(3) based on the disentangled representation space V and S .

As shown in Figure 4, the overall process includes feeding images x_0, x_1, x_2 randomly selected from the source domain G . into identity-specific and domain-specific encoders to obtain disentangled representations s_0, s_1, s_2 and v_0, v_1, v_2 via adversarial learning. Then backdoor adjustment is performed based on these representations to further train the encoders f_S and f_V for learning invariant representations.

Identity Adversarial Learning Block. An identity-aware encoder f_S is adopted to extract identity-specific factors. Then, a classifier \mathcal{C}_S is used to identify the ID label for a given person image x_i . The cross-entropy loss with label smoothing [56] is calculated to train the encoder f_S , which is defined as:

$$\mathcal{L}_{id}^s = - \sum_{i=1}^N \log P(Y = y_i; \mathcal{C}_S(f_S(x_i))) \quad (4)$$

where θ_S is the parameters of f_S , \mathcal{C}_S is the identity classifier. y_i is the labeled person identity of x_i .

To exclude all the domain information from identity-specific factors, a domain classifier \mathcal{C}_V is adopted for adversarial

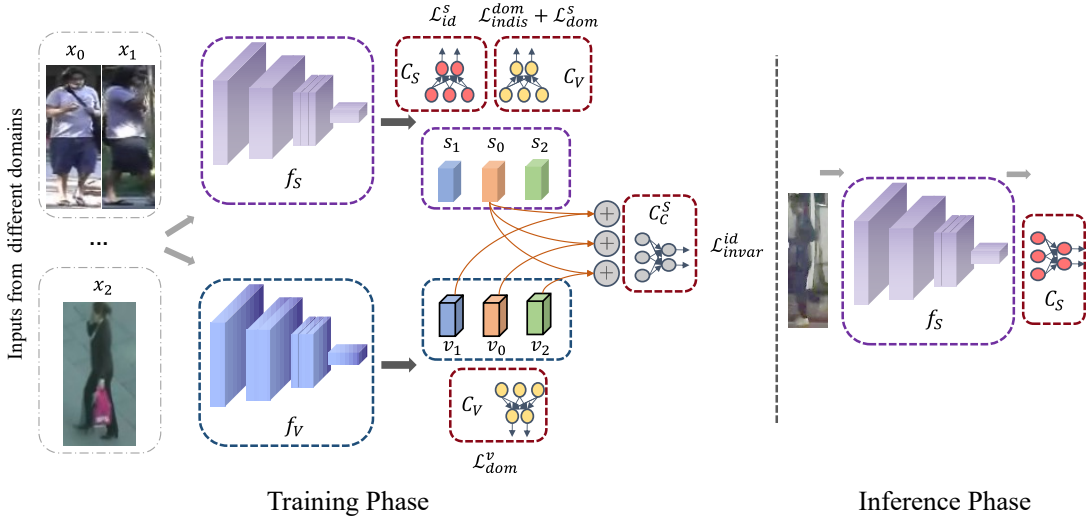


Fig. 4. **Schematic description of the proposed approach.** x_0, x_1, x_2 : Three images from one mini-batch. f_S, f_V : encoders of identity-specific and domain-specific factors. s, v : identity-specific and domain-specific factors represented in latent space. C_S, C_V, C_C : classifiers for identity-specific factors, domain-specific factors, and concatenated vectors. \oplus : concatenation of two latent vectors

learning. One promising way is to use the gradient reversal layer (GRL) technique in DANN [31] to train the encoder f_S and classifier C_V simultaneously, where a misclassification loss is adopted to force an image not to be classified in its true domain class. However, a desirable disentangled representation should be “indistinguishability”, rather than “misclassification”, which means classifying the input into all the domains equiprobably. Hence, we adopt a loss of maximum entropy (minimization of negative entropy [52]) termed the domain-indistinguishability loss as follows.

$$\mathcal{L}_{indis}^{dom} = -\mathcal{H}(D|S), \quad (5)$$

where \mathcal{H} is the entropy to measure the uncertainty of the predicted domain class given identity-specific factors, *i.e.*,

$$\mathcal{H}(D|S) = -\sum_{i=1}^N P(D = d_i; C_V(f_S(x_i))) \cdot \log P(D = d_i; C_V(f_S(x_i))), \quad (6)$$

by which the extracted identity-specific features are required to reduce the domain information as less as possible.

As a result, the parameters θ_S of the identity-aware encoder f_S are optimized by jointly minimizing the identity-classification loss and the domain-indistinguishability loss. The overall objective function of identity adversarial learning is as follows:

$$\min_{\theta_S} \mathcal{L}_{id}^S + \lambda_1 \mathcal{L}_{indis}^{dom}, \quad (7)$$

where λ_1 is a hyper-parameter to balance the trade-off between two losses.

Domain Factors Learning Block. This block aims to extract domain-specific factors from person images x_i .

The domain classification loss \mathcal{L}_{dom}^v is defined as,

$$\mathcal{L}_{dom}^v = -\sum_{i=1}^N \log P(D = d_i; C_V(f_V(x_i))), \quad (8)$$

where d_i is the domain label of image x_i . The identity-indistinguishability loss \mathcal{L}_{indis}^{id} is similar to Eq.(6).

Backdoor Adjustment Block. With the disentangled representations learned from MDDAN, we can implement the backdoor adjustment. Given samples $\{x_i\}_{i=1}^N$, we first feed them to f_S and f_V to obtain $\{v_i\}_{i=1}^N$ and $\{s_i\}_{i=1}^N$. Then we follow two similar assumptions in [50].

(i) $P(v_i) = 1/|V|$, where we assume a uniform prior for the adjusted domain-specific factors.

(ii) $P(Y|S = s_i, V = v_k) = P(Y|s_i \oplus v_k)$, where \oplus denotes vector concatenation.

Based on the above assumption, the overall backdoor adjustment is as follows:

$$P(Y|do(S = s_i)) = \frac{1}{|V|} \sum_{k=1}^{|V|} P(Y|s_i \oplus v_k) \quad (9)$$

Here, to traverse all possible V , we propose 4 approximate implementations through random sampling over the feature space V .

- *K*-Random. For each x_i , we randomly select K different domain-specific factors $\{v_k\}_{k=1}^K$ where $k \neq i$.
- *K*-Hardest. For each x_i , we select K domain-specific factors $\{v_k\}_{k=1}^K$ that are the most dissimilar to v_i .
- *K*-Mixup. For each x_i , we can create more domain-specific factors by mixup [57], [58]. We generate K mixed sample feature \tilde{v} by interpolation of two randomly selected features (a pair $\langle v_k, v'_k \rangle$), denoted by

$$\tilde{v} = \alpha v_k + (1 - \alpha)v'_k, \quad (10)$$

where $\alpha \in [0, 1]$ controls the degree of interpolation and we empirically set $\alpha = 0.5$ in our experiments.

- *K*-MixHard. For each x_i , we firstly select K domain-specific factors $\{v_k\}_{k=1}^K$ least like v_i and generate K mixed features by randomly interpolating these factors.

Then we can approximate the backdoor adjustment by

$$P(Y|do(S = s_i)) = \frac{1}{K} \sum_{k=1}^K P(Y|s_i \oplus v_k) \quad (11)$$

Taking into account the constant $1/K$, the final loss function is as follows.

$$\mathcal{L}_{invar}^{id} = - \sum_{i=1}^N \sum_{k=1}^K \log P(Y = y_i; \mathcal{C}_C^S(s_i \oplus v_k)), \quad (12)$$

where the \mathcal{C}_C^S is a classifier for the concatenated feature vectors.

E. Model Summary

Finally, given the parameters ϕ_S, ϕ_V of the classifiers $\mathcal{C}_S, \mathcal{C}_V$, the total loss function is summarized as follows.

$$\min_{\phi_S, \phi_V} \mathcal{L}_{id}^s + \mathcal{L}_{dom}^s + \mathcal{L}_{dom}^v. \quad (13)$$

And the overall loss functions for the other components are defined as

$$\begin{aligned} \min_{\theta_S, \phi_C^S} \mathcal{L}_{id}^s + \lambda_1 \mathcal{L}_{indis}^{dom} + \lambda_2 \mathcal{L}_{invar}^{id}, \\ \min_{\theta_V, \phi_C^V} \mathcal{L}_{dom}^v + \lambda_3 \mathcal{L}_{invar}^{id}, \end{aligned} \quad (14)$$

where ϕ_C^S, ϕ_C^V are parameters of classifiers \mathcal{C}_C^S and \mathcal{C}_C^V respectively. With the above components, each mini-batch training process is divided into two phases. In Phase I, the encoders f_S^V and f_V as well as the augmented data classifiers \mathcal{C}_C^S and \mathcal{C}_C^V are trained by Eq.(14), while $\mathcal{C}_S, \mathcal{C}_V$ are fixed. Then in Phase II, $\mathcal{C}_S, \mathcal{C}_V$ are trained by Eq.(13), while other components are fixed.

F. Model Analysis

In this section, we first give a theoretical analysis of MDDAN. Then, we state the differences between MDDAN and other adversarial leaning-based methods. Finally, we discuss the proposed BA block in comparison with other causal representation methods.

1) Theoretical characteristics of MDDAN:

Lemma 3.1: Let τ denote one of the source domains, s^j are identity-specific factors of images from the j -th domain. Let $p(s^j|\tau = i)$ be the class-conditional density function of the j -th domain given domain information $\tau = i$. It can be shown that carrying out MDDAN will lead to

$$p(s^j|\tau = i) = p_j(s^j), \forall s^j, i = 1, \dots, G. \quad (15)$$

It indicates that in the latent space of identity-specific representation, the probability density will be invariant to different domains. Its class-conditional density function given any domains (e.g., $p(s^j|\tau = i)$) is just equal to its prior density function value in its own domain (e.g., $p_j(s^j)$), but not depends on the domain variable τ .

Proof 3.1: Referring to [5], we can prove the Lemma 3.1. All the analyses are conducted in the shared identity-specific representation space. We first prove the following lemma.

Lemma 3.2: When MDDAN is carried out to perform adversarial learning in Eq.(6), given any identity-specific representation s^j of an image from domain $\tau = i$, the conditional probability of any $\tau = i$ given s^j will be equal to $1/G$, that is, for any $i = 1, \dots, G$, we have $p(\tau = i|s^j) = 1/G$.

Proof 3.2: Here we slightly abuse the notation: omitting the domain classifier \mathcal{C}_V and $p(k|s^j)$ is equivalent to $p(\tau = k|s^j)$. MDDAN is defined as follows.

$$\begin{aligned} \max - \sum_{k=1}^G p(\tau = k|s^j) \log p(\tau = k|s^j), \\ \text{s.t. } \sum_{k=1}^G p(\tau = k|s^j) = 1; p(\tau = k|s^j) \geq 0, \forall k. \end{aligned} \quad (16)$$

Let $\mathcal{H}(p_k) = p_k \log p_k$, where $p_k = p(\tau = k|s^j)$. We simplify the above optimization problem as

$$\min \sum_{k=1}^G \mathcal{H}(p_k), \text{ s.t. } \sum_{k=1}^G p_k = 1; p_k \geq 0, \forall k, \quad (17)$$

where $\mathcal{H}(p_k)$ is convex as we have $\mathcal{H}''(p_k) = \frac{1}{p_k \ln 2} > 0$. The sum of convex functions $\sum_{k=1}^G \mathcal{H}(p_k)$ is also a convex function. That is, this problem is a convex optimization problem. To prove the lemma, it is now equivalent to show that the minimum value of this convex optimization problem is obtained when $p_1 = p_2 = \dots = p_G = 1/G$.

We use *augmented Lagrangian method* to solve the problem, where the Lagrange function is defined as

$$L(p, \lambda) = \sum_{k=1}^G p_k \log p_k + \lambda \left(\sum_{k=1}^G p_k - 1 \right). \quad (18)$$

We take partial derivatives for each p_k and get

$$\frac{\partial L(p, \lambda)}{\partial p_k} = \log p_k + \frac{1}{\ln 2} + \lambda = 0. \quad (19)$$

Then we have $p_k = 2^{-\lambda-1/\ln 2}$. As $\sum_{k=1}^G p_k = 1$, we have $G * 2^{-\lambda-1/\ln 2} = 1$, and thus $p_k = 1/G, i = 1, 2, \dots, G$. Since the local minimum of the convex function is the global minimum, when $p_1 = p_2 = \dots = p_G = 1/G$, $\sum_{k=1}^G \mathcal{H}(p_k)$ achieves the minimum value, $\log \frac{1}{G}$. In other words, when MDDAN is carried out and achieves the maximum uncertainty, for all $i = 1, \dots, G$, we have $p(\tau = i|s^j) = 1/G$.

Now we are ready to prove Lemma 1. We can calculate any domain τ 's conditional probability given s^j , which is

$$p(\tau = i|s^j) = \frac{p(s^j|\tau = i)p(\tau = i)}{p_j(s^j)}, \forall s^j; i = 1, \dots, G, \quad (20)$$

where $p(s^j|\tau = i)$ denotes the conditional probability of s^j given domain information $\tau = i$, $p_j(s^j)$ denotes the probability function of the identity-specific representation in its domain $\tau = j$, and $p(\tau = i)$ is the prior probability of domain classes $\tau = i$. Without generality, we set equal prior probability for each domain, namely $p(\tau = i) = 1/G$. Further, from the Lemma 3.1 we know that, optimizing MDDAN leads to $p(\tau = i|s^j) = 1/G$ for all $i = 1, \dots, G$. Hence, Eq.(20) becomes

$$1/G = \frac{p(\mathbf{s}^j | \tau = i)1/G}{p_j(\mathbf{s}^j)}, \forall \mathbf{s}^j; i = 1, \dots, G, \quad (21)$$

$$\Rightarrow p(\mathbf{s}^j | \tau = i) = p_j(\mathbf{s}^j), \forall \mathbf{s}^j; i = 1, \dots, G,$$

thus completing the proof.

Lemma 3.3: From the view of information theory, MD-DAN is minimizing the mutual information between identity-specific factors S and domain information variables τ , namely $\min \mathcal{I}(S, \tau)$.

Proof 3.3:

Minimizing the mutual information between the identity-specific factors S and the domain information variables τ is defined as

$$\begin{aligned} \min \mathcal{I}(S, \tau) &= \min \mathcal{H}(\tau) - \mathcal{H}(\tau|S) \\ &= \min -\mathcal{H}(\tau|S) \\ &= \max \mathcal{H}(\tau|S) \end{aligned} \quad (22)$$

The second line is derived since the entropy of the domain distribution $\mathcal{H}(\tau)$ is not related to our optimization, which is only related to the statistics of the dataset. That is, our MD-DAN is essentially minimizing mutual information between identity-specific factors and domain information.

2) *Comparison with other adversarial learning-based methods:* Here we discuss similar studies DANN [31], DDAN [32] and CaNE [33], which also use adversarial training to reduce domain divergence or nuisance divergence. There are three differences between our methods and them: (i) The **implementation strategies** are different. Given n domains, DANN [31] needs n binary classifiers to check which domain one image belongs to. DDAN [32] selects one central domain, using one binary classifier to check if one image belongs to the central (1) or peripheral (0) domain. CaNE [33] implements adversarial training in nuisance attributes (camera ID and video timestamps), where a reweighted form of negative entropy is implemented to take into account class imbalance problems. We directly use entropy maximization with one multi-domain classifier, which extends the assumption of binary classification in DANN. (ii) The **roles** of adversarial learning are different. In our work, MDDAN is first performed to obtain an initial disentangled representation of the identity/domain-specific factors. Then, the MDDAN and BA blocks are implemented jointly to further optimize the disentangled representation. While other related work only uses adversarial training to enhance the invariance of learned representations to some nuisances.

3) *Comparison with disentanglement-based methods:*

Compared to [52], our method has mainly three differences (1) **Setting**. [52] focus on domain adaptation, which has only two domains, i.e., the source domain and the target domain and a set of images in the target domain can be used for domain adaptation during the training phase. Ours are domain generalization, which has multiple domains and the target domain is unseen during training. (2) **Methodologies**. [52] has one decoder and uses the Evidence Lower Bound (ELBO) loss for training, which is not required for MDDAN. Furthermore, [52] uses traditional adversarial training + GRL to

exclude domain-specific information, and we use the domain-indistinguishability loss. (3) We provide **mathematical explanations**. Firstly, we prove that the global optimal solution of MDDAN will lead to the independence between identity-specific and domain-specific factors (Lemma 3.1). Secondly, we prove that MDDAN is equivalent to minimizing mutual information between identity and domain factors (Lemma 3.3).

There are also some other works on domain adaptation contributing to distinguishing domain-specific and domain-invariant features [59], however, [59] first estimates pseudo-labels for the examples in the target domain using the existing unsupervised domain adaptation algorithm and then learns the normalization layers for source and target domains separately. Though UDA-based methods improve the performance of cross-domain ReID to a certain extent, most of them require a large amount of unlabeled target data for model retraining, which is unrealistic for DG ReID.

4) *Comparison with other causal representation learning methods:* DIR-Reid has a similar causal graph with [46], [47], [50]. [46], [47], [50] describe the causal mechanism in various visual tasks, while the elements in the SCM and the implementation details are entirely different. (i) *Elements in the SCM*. The main differences are list in Table. I. As far as we know, it is the first attempt to use backdoor adjustment in the disentangled feature space (identity-specific and domain-specific feature spaces). (ii) *Implementation details*. the implementation of [47] is based on front-door adjustment. The implementation of [46] is simple yet efficient: they concatenate the causal feature with the features of all the confounders and then use the concatenated feature to predict the label. [50] propose three kinds of implementations of backdoor adjustment, where the class-wise adjustment is most relevant to us. They concatenate the probabilistic combination of pretraining features of all classes with the causal feature to predict the label of the causal feature. The BA block in our work also implements backdoor adjustment by feature concatenation with a number of selected domain-specific feature vectors. Since it is untractable to get a well-defined confounder dictionary [46] or pretraining features for all class [50]. It is natural to simply adopt the domain feature as the confounder dictionary⁵. However, it works poorly (the second row in Table VI), which indicates that it is indispensable to disentangle the identity-specific factors and domain-specific factors and use the proposed approximate implementations.

IV. EXPERIMENTS

A. Datasets and Settings

Following [9], [28], we evaluate the DIR-ReID with multiple data sources (MS), where source domains cover five large-scale ReID datasets, including CUHK02 [60], CUHK03 [61], Market1501 [7], DukeMTMC-ReID [62], CUHK-SYSU PersonSearch [63]. The details of MS are summarized in Table II. The unseen test domains are VIPeR [64], PRID [54], QMUL GRID [8] and i-LIDS [65]. We follow the single-shot setting, where the number of probe/gallery images is summarized

⁵For each domain, the average of all the images' features will serve as the domain's feature. Namely, the confounder dictionary has G items.

| | Field | Causal | Effect | Confounder |
|---------------|-----------------------|-----------------------|------------------|--------------------|
| DIC [47] | Image captioning | Image | Caption | Pretrained dataset |
| VC R-CNN [46] | Image captioning, VQA | Object representation | Object label | Context objects |
| IFSL [50] | Few shot learning | Image | Label | Pretrain knowledge |
| BA (ours) | Domain generalization | Semantic factors | Pedestrian label | Variation factors |

TABLE I
ITEMS IN THE SCM

| Collection | Dataset | IDs | Images |
|------------|----------------|--------|--------|
| | CUHK02 | 1,816 | 7,264 |
| | CUHK03 | 1,467 | 14,097 |
| MS | DukeMTMC-Re-Id | 1,812 | 36,411 |
| | Market-1501 | 1,501 | 29,419 |
| | CUHK-SYSU | 11,934 | 34,547 |

TABLE II

TRAINING DATASETS STATISTICS. ALL THE IMAGES IN THESE DATASETS, REGARDLESS OF THEIR ORIGINAL TRAIN/TEST SPLITS, ARE USED FOR MODEL TRAINING.

| Dataset | Probe | | Gallery | |
|---------|---------|----------|---------|----------|
| | Pr. IDs | Pr. Imgs | Ga. IDs | Ga. imgs |
| PRID | 100 | 100 | 649 | 649 |
| GRID | 125 | 125 | 1025 | 1,025 |
| VIPeR | 316 | 316 | 316 | 316 |
| i-LIDS | 60 | 60 | 60 | 60 |

TABLE III

TESTING DATASETS STATISTICS.

in Table III. The average rank-k (R-k) accuracy and mean Average Precision (mAP) over 10 random splits are reported based on the evaluation protocol. In this way, we simulate the real-world setting in which a ReID model is trained with all the public datasets and evaluate the generalization capability to unseen domains. Detailed evaluation protocols are as follows.

GRID [8] contains 250 probe images and 250 true match images of the probes in the gallery. Also, there are a total of 775 additional images that do not belong to any of the probes. We randomly remove 125 probe images. The remaining 125 probe images and 1025(775 + 250) images in the gallery are used for testing.

i-LIDS [65] has two versions, images and sequences. The former is used in our experiments. It involves 300 different pairs of pedestrians observed in two disjoint camera views 1 and 2 in open public spaces. We randomly select 60 pedestrian pairs, two images per pair are randomly selected as probe image and gallery image, respectively.

PRID2011 [54] has single shot and multishot versions. We use the former in our experiments. The single-shot version has two camera views *A* and *B*, which capture 385 and 749 pedestrians, respectively. Only 200 pedestrians appear in both views. During the evaluation, 100 randomly identities presented in both views are selected, the remaining 100 identities in view *A* constitute the probe set, and the remaining 649 identities in view *B* constitute the gallery set.

VIPeR [64] contains 632 pairs of pedestrian images. Each

pair contains two images of the same individual seen from different camera views 1 and 2. Each pair of images was taken from an arbitrary viewpoint under varying illumination conditions. To compare to other methods, we randomly select half of these identities from camera view 1 as probe images and their matched images in view 2 as gallery images.

B. Implementation Details

Following previous generalizable person ReID methods, we use MobileNetV2 [66] as the domain-specific encoder f_V and use MobileNetV2 with IN layer [67] as identity-specific encoder f_S . Our classifiers $\mathcal{C}_S, \mathcal{C}_V, \mathcal{C}_C^S, \mathcal{C}_C^V$ are simply composed of a single fully-connected layer. Images are resized to 256×128 and the training batch size is set to 128. Random cropping, random flipping, and color jitter are applied as data augmentations. The label smoothing parameter is 0.1. SGD is used to train all components from scratch with a learning rate of 0.02 and a momentum of 0.9. The training process includes 150 epochs and the learning rate is divided by 10 after 100 epochs. At test time, DIR-ReID only involves identity-specific encoder f_S , which is of a comparable network size to most ReID methods. The tradeoff weights are set to $\lambda_2 = 0.1$ and $\lambda_1 = \lambda_3 = \lambda_4 = 1$ empirically.

C. Comparisons Against State-of-the-art

Comparison with single domain methods. Many supervised methods report high performance on large-scale benchmarks, but their performance is still poor on small-scale. We select 6 representative models (labeled as ‘S’ in Table IV) in comparisons, which are trained with the data splits in the target datasets. Although data from the target domain are inaccessible for DIR-ReID, it achieves competitive or better performance on all four benchmarks, which indicates that sufficient source data and our model based on domain invariance learning can alleviate the need for data from the target domain.

Comparison with DG methods. Then, we compare DIR-ReID with existing methods on generalizable person ReID. As far as we know, there are a few publications focusing on person ReID generalization problem, including DIMN [9], DualNorm [28], [73] and DDAN [32]. From the third row in Table IV, DIR-ReID has achieved the best performance in terms of mAP against other SOTA DG-ReID methods. Although our method falls behind others on the i-LIDS and the GRID datasets in terms of Rank-5 and Rank-10, the DIR-ReID obtains the best Rank-1 performance on three of four datasets. Interestingly, methods such as SNR [29] and AugMining [73] perform very well in i-LIDS, while having low performance in

| Methods | Type | Source | VIPeR (V) | | | | PRID (P) | | | | GRID (G) | | | | i-LIDS (I) | | | |
|-----------------|------|--------|-------------|-------------|-------------|-------------|-------------|-------------|-------------|-------------|-------------|-------------|-------------|-------------|-------------|-------------|-------------|-------------|
| | | | R-1 | R-5 | R-10 | mAP | R-1 | R-5 | R-10 | mAP | R-1 | R-5 | R-10 | mAP | R-1 | R-5 | R-10 | mAP |
| DeepRank [68] | S | Target | 38.4 | 69.2 | 81.3 | - | - | - | - | - | - | - | - | - | - | - | - | - |
| DNS [69] | S | Target | 42.3 | 71.5 | 82.9 | - | 29.8 | 52.9 | 66.0 | - | - | - | - | - | - | - | - | - |
| MTDnet [70] | S | Target | 47.5 | 73.1 | 82.6 | - | 32.0 | 51.0 | 62.0 | - | - | - | - | - | 58.4 | 80.4 | 87.3 | - |
| JLML [69] | S | Target | 50.2 | 74.2 | 84.3 | - | - | - | - | - | 37.5 | 61.4 | 69.4 | - | - | - | - | - |
| SSM [71] | S | Target | 53.7 | - | 91.5 | - | - | - | - | - | 27.2 | - | 61.2 | - | - | - | - | - |
| SpindleNet [72] | S | Target | 58.3 | 74.1 | 83.2 | - | 67.0 | 89.0 | 89.0 | - | - | - | - | - | 66.3 | 86.6 | 91.8 | - |
| AugMining [73] | DG | MS | 49.8 | 70.8 | 77.0 | - | 34.3 | 56.2 | 65.7 | - | 46.6 | 67.5 | 76.1 | - | 76.3 | 93.0 | 95.3 | - |
| DIMN [9] | DG | MS | 51.2 | 70.2 | 76.0 | 60.1 | 39.2 | 67.0 | 76.7 | 52.0 | 29.3 | 53.3 | 65.8 | 41.1 | 70.2 | 89.7 | 94.5 | 78.4 |
| DualNorm [28] | DG | MS | 53.9 | 62.5 | 75.3 | 58.0 | 60.4 | 73.6 | 84.8 | 64.9 | 41.4 | 47.4 | 64.7 | 45.7 | 74.8 | 82.0 | 91.5 | 78.5 |
| SNR [29] | DG | MS | 52.9 | - | - | 61.3 | 52.1 | - | - | 66.5 | 40.2 | - | - | 47.7 | 84.1 | - | - | 89.9 |
| DDAN [32] | DG | MS | 56.5 | 65.6 | 76.3 | 60.8 | 62.9 | 74.2 | 85.3 | 67.5 | 46.2 | 55.4 | 68.0 | 50.9 | 78.0 | 85.7 | 93.2 | 81.2 |
| DIR-ReID | DG | MS | 58.5 | 76.9 | 83.3 | 67.0 | 69.7 | 85.8 | 91.0 | 77.1 | 48.2 | 67.1 | 76.3 | 57.6 | 79.0 | 94.8 | 97.2 | 83.4 |

TABLE IV

COMPARISONS AGAINST STATE-OF-THE-ART METHODS. 'S': SINGLE DOMAIN, 'DG': DOMAIN GENERALIZATION, 'M': MARKET1501, 'D': DUKEMTMC-REID, 'COMB': THE COMBINATION OF VIPeR, PRID, CUHK01, I-LIDS, AND CAVIAR DATASETS. 'C3': CUHK03, '-': NO REPORT. 1st AND 2^{ed} HIGHEST ACCURACY ARE INDICATED BY BLUE AND RED COLOR.

| Method | Cross-domain Re-ID (single-source DG) | | | | | | | |
|----------------|---------------------------------------|-------------|-------------|-------------|-------------|-------------|-------------|-------------|
| | Market-Duke | | | | Duke-Market | | | |
| | R-1 | R-5 | R-10 | mAP | R-1 | R-5 | R-10 | mAP |
| IBN-Net [74] | 43.7 | 59.1 | 65.2 | 24.3 | 50.7 | 69.1 | 76.3 | 23.5 |
| OSNet [75] | 44.7 | 59.6 | 65.4 | 25.9 | 52.2 | 67.5 | 74.7 | 24.0 |
| OSNet-IBN [75] | 47.9 | 62.7 | 68.2 | 27.6 | 57.8 | 74.0 | 79.5 | 27.4 |
| CrossGrad [76] | 48.5 | 63.5 | 69.5 | 27.1 | 56.7 | 73.5 | 79.5 | 26.3 |
| QACConv [77] | 48.8 | - | - | 28.7 | 58.6 | - | - | 27.6 |
| L2A-OT [78] | 50.1 | 64.5 | 70.1 | 29.2 | 63.8 | 80.2 | 84.6 | 30.2 |
| OSNet-AIN [75] | 52.4 | 66.1 | 71.2 | 30.5 | 61.0 | 77.0 | 82.5 | 30.6 |
| SNR [29] | 55.1 | - | - | 33.6 | 66.7 | - | - | 33.9 |
| DIR-ReID | 54.5 | 66.8 | 72.5 | 33.0 | 68.2 | 80.7 | 86.0 | 35.2 |

TABLE V

PERFORMANCE (%) COMPARISON WITH THE STATE-OF-THE-ARTS ON THE CROSS-DOMAIN REID PROBLEM. 1st AND 2^{ed} HIGHEST ACCURACY ARE INDICATED BY BLUE AND RED COLOR.

other datasets, suggesting the unstable generalization abilities of their models. To further measure the generalization ability, we adopt the worst-domain accuracy (WDA) proposed in [79] for a comparison. From Table IV, we can find that our DIR-ReID achieves the highest WDA value with 47.8% rank-1 accuracy, which demonstrates the superior generalization ability of our model.

Comparison with cross-domain Re-ID methods.

To further evaluate the generalization ability of our approach, we also perform cross-domain ReID tests with two large-scale datasets, *i.e.*, Market1501 and DukeMTMC. The experimental results are presented in Table V ("Market1501→DukeMTMC" indicates that Market-1501 is a labeled source domain and DukeMTMC-ReID is an unseen target domain). It is different from the settings in UDA methods, all models in our comparisons only use the source data for training without any model adaptations in the target domain. The setting of cross-domain Re-ID is challenging for us because there is only one source domain. Thus we consider each camera view as a single domain for training the MDDAN block. As the camera views in the same dataset may share similar imaging characteristics, *e.g.*, background environments, and resolutions, the variations of domain-specific factors may be smaller within a single dataset than that of multiple data sources. Despite this, Table V shows that our DIR-ReID framework achieved comparable performance on both settings. It indicates that, even with small domain variations, DIR-ReID can improve the generalization capability.

It is noted that DIR-ReID still has a large margin with current UDA methods (*e.g.*, MMT [26] achieves more than 75% rank 1 accuracy in the "Market-to-Duke" dataset setting, which is much superior to current DG methods). DIR-ReID does not need any model adaptations with the data of the target domain, which significantly reduces the costs of large-scale data collections in practical deployments of ReID models.

D. Ablation Studies

There are two main components in the proposed DIR-ReID: the MDDAN block and the BA block. Here, we first analyze the effectiveness of each block respectively, then demonstrate their contributions to the final performance of the whole DIR-ReID model.

Effectiveness of MDDAN. The superiority of MDDAN is verified by comparisons with the dual DANN [31] block. The latter means inserting the GRL layers between f_S, C_V and f_V, C_S . Simultaneously, the dual DANN block replaces the maximum entropy loss in MDDAN with the maximum misclassification loss. The results are shown in Table VI. The dual DANN method only has an improvement with average 1.1 points over 4 test datasets in comparison with the baseline, while our MDDAN block leads to significant improvements.

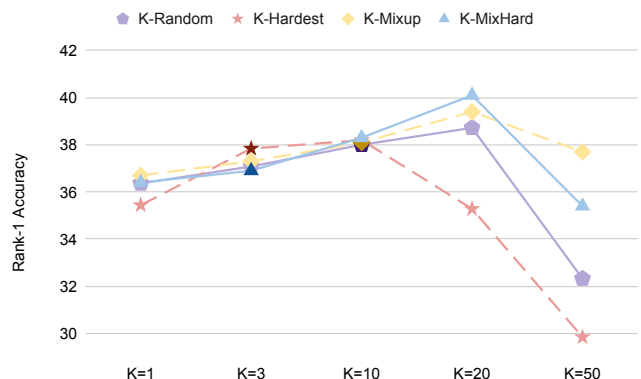


Fig. 5. Ablation study on BA block. The metric is the rank-1 accuracy on the GRID dataset. Considering the expensive cost of training with five datasets, all the models here are trained on three datasets, *i.e.*, Market-1501, CUHK02 and CUHK03.

| | PRID | VIPeR | i-LIDS | GRID |
|-------------------------------|------|-------|--------|------|
| Baseline (DualNorm [28]) | 38.9 | 54.0 | 64.3 | 34.4 |
| w/ Dual DANN [31] | 41.0 | 53.3 | 66.2 | 35.4 |
| Improvements↑ | 2.1 | -0.7 | 1.9 | 1.0 |
| w/ Confounder Dict [46], [50] | 39.4 | 54.7 | 65.8 | 35.9 |
| Improvements↑ | 0.5 | 0.7 | 1.5 | 1.5 |
| w/ MDDAN | 42.7 | 56.5 | 65.7 | 36.6 |
| Improvements↑ | 3.8 | 2.5 | 1.4 | 2.2 |
| w/ BA | 43.8 | 61.4 | 68.2 | 40.2 |
| Improvements↑ | 4.9 | 7.4 | 3.9 | 5.8 |
| w/ Triplet Loss | 44.6 | 62.7 | 68.9 | 41.4 |
| Improvements↑ | 5.7 | 8.7 | 4.6 | 7.0 |

TABLE VI

ABLATION STUDIES ON THREE DIFFERENT BLOCKS: DUAL DANN BLOCK, CONFOUNDER DICTIONARY BLOCK, THE PROPOSED MDDAN BLOCK AND THE BA BLOCK. THE METRIC IS RANK-1 ACCURACY. MODELS HERE ARE ALL TRAINED ON THREE DATASETS, INCLUDING MARKET-1501, CUHK02 AND CUHK03. THE IMPROVEMENTS DENOTE THE DIFFERENCE FROM THE BASELINE.

Effectiveness of BA block. Firstly we compare the proposed BA block with Confounder Dict, which imitates similar backdoor adjustment-based methods [46], [50]. The difference between Confounder Dict and DIR-ReID is the source of variation factors. Specifically, Confounder Dict uses a pretrained MobileNetV2 (pretrained in ImageNet) to extract all the features of the data points. The average feature of the images in domain g will serve as its confounder feature v_g and $\{v_g\}_{g=1}^G$ will serve as domain-specific factors. Then BA block can be executed by concatenating the identity-specific factors extract by f_S and the pretrained domain-specific factors. The results are shown in Table VI. The confounder Dict is inferior to DIR-ReID and we believe there are two reasons: (i) The pretrained MobileNetV2 cannot extract the proper factors in surveillance scenarios *e.g.*, backgrounds and illumination conditions. (ii) The number of confounder features G is small and cannot cover the variation space at all. On the contrary, the DIR-ReID trains a f_V to extract variation factors for each person image to obtain specific domain factors. Hence it is more potential to approximate the variation space and finish the backdoor adjustment. We also compare four different implementations of BA and the results are shown in Fig. 5. K -Random is the simplest method while it works well, attaining 38.72% rank 1 accuracy when $K = 20$. K -MixHard outperforms other methods and attains 40.16% rank 1 accuracy, which verified the importance of mixup for data augmentation. However, as we increase the value of K , the performance will not be improved.

Ablation study of different blocks. To evaluate the contribution of each component, we gradually add the MDDAN and the BA to the baseline, and the overall ablation studies are reported in Table VI. The MDDAN improves the rank-1 accuracy from 34.4% to 36.6% in the GRID dataset. The results in PRID, VIPeR, and i-LIDS datasets are consistently improved, which validates that the MDDAN removes some of the domain-specific information from the identity-specific representations and yields consistent generalization performance improvements. The BA provides greater improvement gains on three test datasets. It validates that BA can exclude domain-specific information efficiently. Besides, We conduct

| | PRID | VIPeR | i-LIDS | GRID | Avg |
|---|------|-------|--------|------|-------|
| Baseline (only \mathcal{L}_{id}^s) | 38.9 | 54.0 | 64.3 | 34.4 | 47.98 |
| MDDAN ($\mathcal{L}_{id}^s + \mathcal{L}_{indis}^{dom}$) | 42.7 | 56.5 | 65.7 | 36.6 | 50.38 |
| \mathcal{L}_{invar}^{id} | 39.1 | 53.7 | 63.2 | 35.2 | 47.80 |
| $\mathcal{L}_{invar}^{id} + \mathcal{L}_{id}^s$ | 39.1 | 54.2 | 64 | 34.8 | 48.03 |
| $\mathcal{L}_{invar}^{id} + \mathcal{L}_{id}^s + \mathcal{L}_{dom}^v$ | 40.0 | 58.2 | 66.7 | 39.6 | 51.13 |
| $\mathcal{L}_{invar}^{id} + \mathcal{L}_{id}^s + \mathcal{L}_{indis}^{dom} + \mathcal{L}_{dom}^v$ | 43.8 | 61.4 | 68.2 | 40.2 | 53.40 |

TABLE VII

ABLATION STUDIES OF EVERY LOSS FUNCTION. THE METRIC IS RANK-1 ACCURACY. MODELS HERE ARE ALL TRAINED ON THREE DATASETS, INCLUDING MARKET-1501, CUHK02, AND CUHK03. THE IMPROVEMENTS DENOTE THE DIFFERENCE FROM THE BASELINE.

an ablation study on the triplet loss, which is also shown able to boost performance, indicating that the metric learning method is orthogonal to our DIR-ReID framework (Last line in Table VI).

Ablation studies of every loss function. A thorough ablation is shown in Table IV-D. Incorporated with $\mathcal{L}_{indis}^{dom}$ for the encoder f_S , the performance of the baseline where only \mathcal{L}_{id}^s for f_S exists can be improved from 47.98% to 50.38%. If we implement BA block only with $\mathcal{C}_C^S, f_S, f_V$ trained by \mathcal{L}_{invar}^{id} or $\mathcal{L}_{invar}^{id} + \mathcal{L}_{id}^s$, namely no constraint on f_V , the performance is similar to the baseline because the feature space is not disentangled well and the backdoor adjustment cannot attain better performance. Once f_V is further trained by \mathcal{L}_{dom}^v , namely, f_V is constrained to contain domain information, the performance gets better. Finally, the $\mathcal{L}_{indis}^{dom}$ is incorporated and f_S is forced to remove domain information, the proposed DIR-ReID attains the best performance in such a disentangled feature space.

We also conduct additional ablation studies on rotated MNIST. The dataset and results are as follows:

E. Ablation studies on Rotated MNIST.

Since the ReID datasets are collected from real surveillance scenarios, complex data variations hinder us from analyzing the characteristics of the proposed model for feature disentanglement. Thus, we performed additional studies on a controlled simple dataset, *i.e.*, the rotated MNIST.

1) *Dataset and Setting:* To verify the capability of the DIR-ReID model to disentangle S and V , we first construct rotated MNIST datasets as follows [80]. 100 images per class (10 classes totally) are randomly sampled from the MNIST training dataset, which is denoted by \mathcal{M}_{0° . We then rotated the images in \mathcal{M}_{0° by 15, 30, 45, 60 and 75 degrees, creating five additional domains. Models are trained in $\{\mathcal{M}_{0^\circ}, \dots, \mathcal{M}_{60^\circ}\}$ and tested on \mathcal{M}_{75° . To plot the latent subspaces directly without applying dimensionality reduction, we restrict the size of latent spaces for S, V to 2 dimensions. In experiments, we train the MDDAN block with an additional reconstruction loss, which is enough to attain an encouraging result.

2) *Architecture and Implementation Details:* The architectures of the encoders, classifiers are shown in Table VIII, Table IX respectively. Our model and the baseline model Dual DANN are trained for 500 epochs and the batch size is set to 100. Adam optimizer is used to train all components from scratch with a learning rate of 0.001. We also use warm-up to

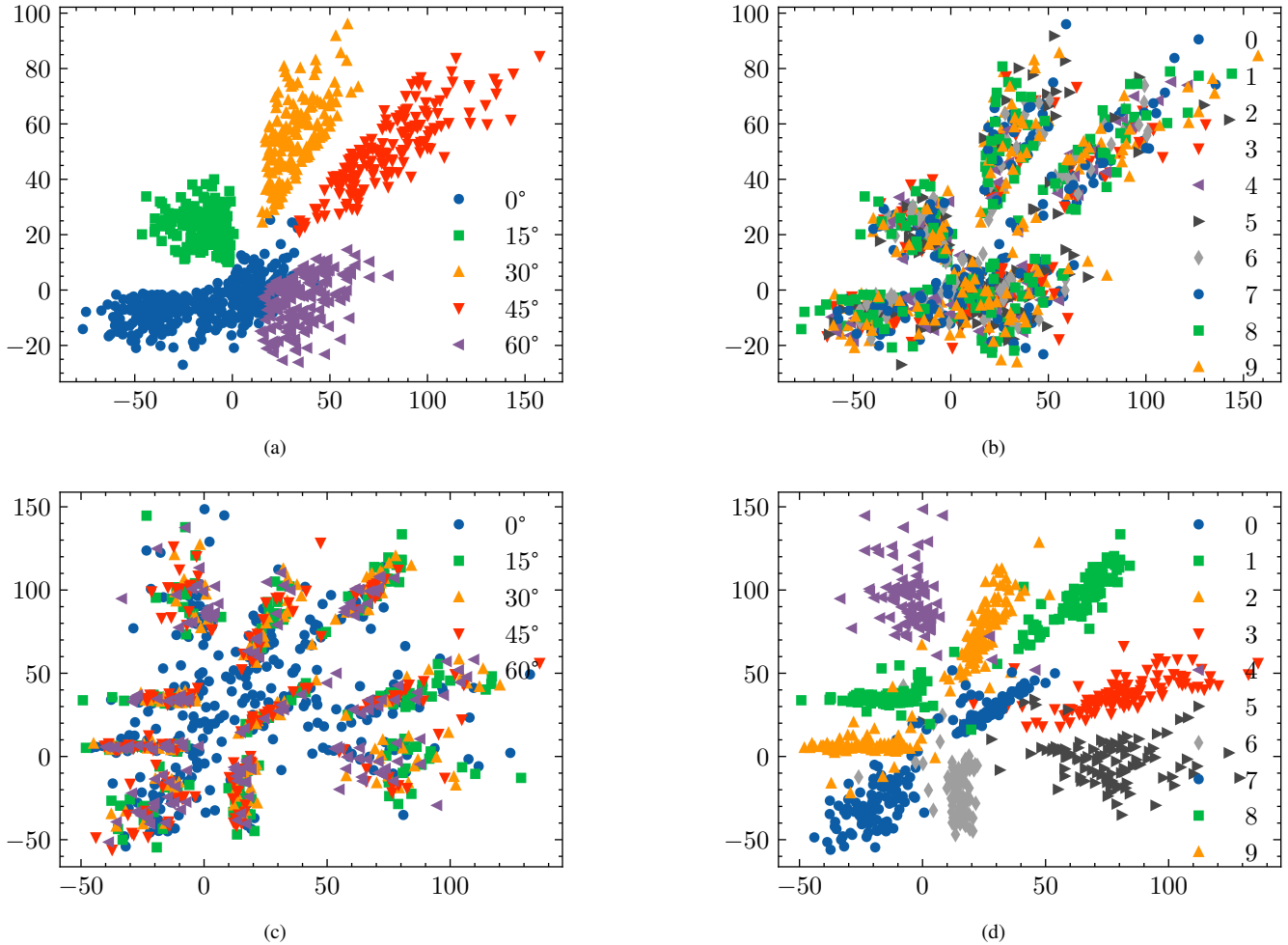


Fig. 6. 2D visualizations of all two latent subspaces. (a,b): v encoded by f_V . (c,d): s encoded by f_S . (a,c) are colored according to their domains and (b,d) are colored according to their classes.

| block | details |
|-------|----------------------------------|
| 1 | Conv2d(32, 5), BatchNorm2d, ReLU |
| 2 | MaxPool2d(2, 2) |
| 3 | Conv2d(64, 5), BatchNorm2d, ReLU |
| 4 | MaxPool2d(2, 2) |
| 5 | Linear(2) |

TABLE VIII

ARCHITECTURE FOR ENCODERS f_S, f_V USED IN THE ABLATION STUDIES ON ROTATED MNIST DATASET. THE PARAMETERS FOR CONV2D ARE OUTPUT CHANNELS AND KERNEL SIZE. THE PARAMETERS FOR MAXPOOL2D ARE KERNEL SIZE AND STRIDE. THE PARAMETER FOR LINEAR IS OUTPUT FEATURES.

| block | details |
|-----------------------|------------------|
| For \mathcal{C}_V | ReLU, Linear(5) |
| For \mathcal{C}_S | ReLU, Linear(10) |
| For \mathcal{C}_C^S | ReLU, Linear(5) |
| For \mathcal{C}_C^V | ReLU, Linear(5) |

TABLE IX

IN THE ABLATION STUDIES ON ROTATED MNIST DATASET: ARCHITECTURE OF CLASSIFIERS FOR ID-SPECIFIC FACTORS, DOMAIN-SPECIFIC FACTORS, AND CONCATENATED VECTORS. THE PARAMETER FOR LINEAR IS OUTPUT FEATURES.

linearly increase the learning rate from 0 to 0.001 during the first 100 epochs of training.

3) *Additional Experimental Results: Analysis of MDDAN.* As shown in Table VI, directly applying the dual GRL block benefits the generalization ability, while the proposed MDDAN improve the test accuracy on \mathcal{M}_{75° dataset by an even more large margin, which is 11.8 points.

Analysis of methods for backdoor adjustment. The comparison results are shown in Fig. 7. Similar to BA for Re-

ID, here K -MixHard attains the most superior performance, which is 61.9% test accuracy.

Ablation study of different blocks. By adding the multi-domain disentangled block and the backdoor adjustment block successively, we improve the generalization accuracy from 46.4% to 58.2% and 61.9% respectively (Table X), showing the effectiveness of the proposed model again.

Visualization analysis. The disentanglement results are visualized in Fig. 6. We can find a correlation between the rotation angle (domain labels) and the learned domain-specific features V in Fig. 6(a), five domains are clustered into five

| Test Accuracy on \mathcal{M}_{75° | |
|---|------|
| Baseline | 46.4 |
| w/ Dual DANN [31] | 53.5 |
| Improvements↑ | 7.1 |
| w/ MDDAN | 58.2 |
| Improvements↑ | 11.8 |
| w/ BA | 61.9 |
| Improvements↑ | 15.5 |

TABLE X

ABLATION STUDY OF THREE DIFFERENT BLOCKS: DUAL GRL BLOCK, OUR MDDAN BLOCK AND THE BA BLOCK. THE REPORTED VALIDATION METRIC IS THE ACCURACY OF THE \mathcal{M}_{75° DATASET. THE BASELINE IS ONLY USING THE ENCODER f_S AND CLASSIFIER C_S .

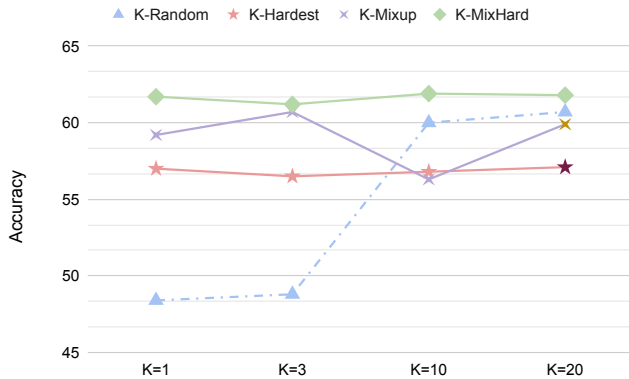


Fig. 7. Ablation study of backdoor adjustment methods. The reported validation metric is the test accuracy of the \mathcal{M}_{70° dataset.

distinct clusters, while in Fig. 6(b) no clustering is visible, which denotes the very weak correlations between V and class labels. By contrast, in Fig. 6(c) no clustering is visible according to the domain labels of rotation angles. But Fig. 6(d) shows ten distinct clusters, where each cluster corresponds to a digit class. From these qualitative results, we conclude that the MDDAN is able to disentangle the information contained in the rotated MNIST dataset, where the learned latent subspaces indeed encode the domain (rotation angles) information and identity (digit classes) information respectively.

V. CONCLUSIONS AND FUTURE WORK

We propose a novel generalizable person ReID approach based on disentanglement and backdoor adjustment from a causal invariance learning framework. Specifically, a MDDAN block is proposed to disentangle identity-specific and domain-specific factors from multi-source ReID training data. We then propose a BA block to learn the interventional distribution and reduce the confounding effects via backdoor adjustment. The comprehensive experimental results show that DIR-ReID achieves state-of-the-art performance.

In future, we can improve the model performance with other regularization techniques. One promising way is to generate realistic images from the latent disentangled representations. The augmented feature vectors are guided by a reconstruction loss, which will further improve the disentanglement of

identity-specific and domain-specific factors. These generated images can also be used for augmenting the training set. Besides, we will seek other methods for better disentanglement performance such as replacing the multi-domain adversarial learning with mutual information minimization [81] or f -divergence maximization [82].

VI. ACKNOWLEDGEMENT

This work is funded by the National Natural Science Foundation of China (Grant No. 62106260), China Postdoctoral Science Foundation (Grant No. 2020M680751), and National Natural Science Foundation of China (62236010, 61721004, and U1803261).

APPENDIX A

DERIVATION OF THE INTERVENTIONAL DISTRIBUTION $P(Y|do(S))$ FOR THE PROPOSED CAUSAL GRAPH

The following proof is similar to [50] with three rules of do -calculus [83]: Insertion/deletion of observations, Action/observation exchange and Insertion/deletion of actions. For consistency, we describe these three rules as follows [50]:

Given a causal directed acyclic graph \mathcal{G} , denote X, Y, Z and W be arbitrary disjoint sets of nodes. We use $\mathcal{G}_{\overline{X}}$ to denote the manipulated graph where all incoming arrows to node X are deleted. Similarly $\mathcal{G}_{\underline{X}}$ represents the graph where outgoing arrows from node X are deleted. Lower case x, y, z and w denote specific values taken by each set of nodes: $X = x, Y = y, Z = z$ and $W = w$. For any interventional distribution compatible with \mathcal{G} , we have the following three rules:

Rule 1 Insertion/deletion of observations:

$$P(y|do(x), z, w) = P(y|do(x), w), \text{ if } (Y \perp\!\!\!\perp Z|X, W)_{\mathcal{G}_{\overline{X}}} \quad (23)$$

Rule 2 Action/observation exchange:

$$P(y|do(x), do(z), w) = P(y|do(x), z, w), \text{ if } (Y \perp\!\!\!\perp Z|X, W)_{\mathcal{G}_{\overline{X}, Z}} \quad (24)$$

Rule 3 Insertion/deletion of actions:

$$P(y|do(x), do(z), w) = P(y|do(x), w), \text{ if } (Y \perp\!\!\!\perp Z|X, W)_{\mathcal{G}_{\overline{X}, Z(W)}}, \quad (25)$$

where $Z(W)$ is a set of nodes in Z that are not ancestors of any W -node in $\mathcal{G}_{\overline{X}}$.

In our causal formulation, the desired interventional distribution $P(Y|do(S = s))$ can be derived by:

$$\begin{aligned} P(Y|do(S)) &= \sum_v P(Y|do(S = s), V = v)P(V = v|do(S = s)) \\ &= \sum_v P(Y|do(S = s), V = v)P(V = v) \\ &= \sum_v P(Y|S = s, V = v)P(V = v), \end{aligned} \quad (26)$$

where line 1 follows the law of total probability; line 2 uses Rule 3 given $S \perp\!\!\!\perp V$ in $\mathcal{G}_{\overline{X}}$; line 3 uses Rule 2 to change the intervention term to observation as $(Y \perp\!\!\!\perp S|V)$ in $\mathcal{G}_{\underline{X}}$.

REFERENCES

- [1] M. Ye, J. Shen, G. Lin, T. Xiang, L. Shao, and S. C. Hoi, "Deep learning for person re-identification: A survey and outlook," *IEEE transactions on pattern analysis and machine intelligence*, vol. 44, no. 6, pp. 2872–2893, 2021.
- [2] Z. Zhang, C. Lan, W. Zeng, X. Jin, and Z. Chen, "Relation-aware global attention for person re-identification," in *Proceedings of the IEEE/CVF Conference on Computer Vision and Pattern Recognition (CVPR)*, June 2020.
- [3] Z. Zheng, X. Yang, Z. Yu, L. Zheng, Y. Yang, and J. Kautz, "Joint discriminative and generative learning for person re-identification," in *Proceedings of the IEEE/CVF Conference on Computer Vision and Pattern Recognition (CVPR)*, June 2019.
- [4] C. Luo, C. Song, and Z. Zhang, "Generalizing person re-identification by camera-aware invariance learning and cross-domain mixup," in *European Conference on Computer Vision (ECCV)*, 2020.
- [5] L. Qi, L. Wang, J. Huo, L. Zhou, Y. Shi, and Y. Gao, "A novel unsupervised camera-aware domain adaptation framework for person re-identification," in *Proceedings of the IEEE/CVF International Conference on Computer Vision (ICCV)*, October 2019.
- [6] C. Eom and B. Ham, "Learning disentangled representation for robust person re-identification," in *Advances in Neural Information Processing Systems*, 2019, pp. 5298–5309.
- [7] L. Zheng, L. Shen, L. Tian, S. Wang, J. Wang, and Q. Tian, "Scalable person re-identification: A benchmark," in *Proceedings of the IEEE International Conference on Computer Vision (ICCV)*, December 2015.
- [8] C. Liu, S. Gong, C. C. Loy, and X. Lin, "Person re-identification: What features are important?" in *European Conference on Computer Vision*. Springer, 2012, pp. 391–401.
- [9] J. Song, Y. Yang, Y.-Z. Song, T. Xiang, and T. M. Hospedales, "Generalizable person re-identification by domain-invariant mapping network," in *Proceedings of the IEEE/CVF Conference on Computer Vision and Pattern Recognition (CVPR)*, June 2019.
- [10] L. G. Neuberg, "Causality: Models, reasoning, and inference," 2003.
- [11] T. Matsukawa, T. Okabe, E. Suzuki, and Y. Sato, "Hierarchical gaussian descriptor for person re-identification," in *Proceedings of the IEEE conference on computer vision and pattern recognition*, 2016, pp. 1363–1372.
- [12] M. Koestinger, M. Hirzer, P. Wohlhart, P. M. Roth, and H. Bischof, "Large scale metric learning from equivalence constraints," in *2012 IEEE conference on computer vision and pattern recognition*. IEEE, 2012, pp. 2288–2295.
- [13] D. Li, X. Chen, Z. Zhang, and K. Huang, "Learning deep context-aware features over body and latent parts for person re-identification," in *Proceedings of the IEEE conference on computer vision and pattern recognition*, 2017, pp. 384–393.
- [14] Y. Sun, L. Zheng, Y. Yang, Q. Tian, and S. Wang, "Beyond part models: Person retrieval with refined part pooling (and a strong convolutional baseline)," in *Proceedings of the European Conference on Computer Vision (ECCV)*, September 2018.
- [15] Z. Zhang, C. Lan, W. Zeng, and Z. Chen, "Densely semantically aligned person re-identification," in *Proceedings of the IEEE/CVF Conference on Computer Vision and Pattern Recognition*, 2019, pp. 667–676.
- [16] C. Song, Y. Huang, W. Ouyang, and L. Wang, "Mask-guided contrastive attention model for person re-identification," in *Proceedings of the IEEE Conference on Computer Vision and Pattern Recognition*, 2018, pp. 1179–1188.
- [17] D. Wu, M. Ye, G. Lin, X. Gao, and J. Shen, "Person re-identification by context-aware part attention and multi-head collaborative learning," *IEEE Transactions on Information Forensics and Security*, vol. 17, pp. 115–126, 2021.
- [18] M. Ye, J. Shen, and L. Shao, "Visible-infrared person re-identification via homogeneous augmented tri-modal learning," *IEEE Transactions on Information Forensics and Security*, vol. 16, pp. 728–739, 2020.
- [19] M. Ye, H. Li, B. Du, J. Shen, L. Shao, and S. C. Hoi, "Collaborative refining for person re-identification with label noise," *IEEE Transactions on Image Processing*, vol. 31, pp. 379–391, 2021.
- [20] M. Ye, C. Chen, J. Shen, and L. Shao, "Dynamic tri-level relation mining with attentive graph for visible infrared re-identification," *IEEE Transactions on Information Forensics and Security*, 2021.
- [21] W. Chen, X. Chen, J. Zhang, and K. Huang, "Beyond triplet loss: a deep quadruplet network for person re-identification," in *Proceedings of the IEEE conference on computer vision and pattern recognition*, 2017, pp. 403–412.
- [22] X. Peng, Y. Li, and S. Kate, "Domain2vec: Domain embedding for unsupervised domain adaptation," *European conference on computer vision (ECCV 2020)*, 2020.
- [23] Y. Huang, Z.-J. Zha, X. Fu, R. Hong, and L. Li, "Real-world person re-identification via degradation invariance learning," in *Proceedings of the IEEE/CVF Conference on Computer Vision and Pattern Recognition*, 2020, pp. 14 084–14 094.
- [24] J. Wang, X. Zhu, S. Gong, and W. Li, "Transferable joint attribute-identity deep learning for unsupervised person re-identification," in *Proceedings of the IEEE Conference on Computer Vision and Pattern Recognition*, 2018, pp. 2275–2284.
- [25] P. Peng, T. Xiang, Y. Wang, M. Pontil, S. Gong, T. Huang, and Y. Tian, "Unsupervised cross-dataset transfer learning for person re-identification," in *Proceedings of the IEEE Conference on Computer Vision and Pattern Recognition (CVPR)*, June 2016.
- [26] Y. Ge, D. Chen, and H. Li, "Mutual mean-teaching: Pseudo label refinery for unsupervised domain adaptation on person re-identification," *arXiv preprint arXiv:2001.01526*, 2020.
- [27] Y. Zhai, Q. Ye, S. Lu, M. Jia, R. Ji, and Y. Tian, "Multiple expert brainstorming for domain adaptive person re-identification," *arXiv preprint arXiv:2007.01546*, 2020.
- [28] J. Jia, Q. Ruan, and T. M. Hospedales, "Frustratingly easy person re-identification: Generalizing person re-id in practice," *arXiv preprint arXiv:1905.03422*, 2019.
- [29] X. Jin, C. Lan, W. Zeng, Z. Chen, and L. Zhang, "Style normalization and restitution for generalizable person re-identification," in *Proceedings of the IEEE/CVF Conference on Computer Vision and Pattern Recognition*, 2020, pp. 3143–3152.
- [30] S. Lin, C.-T. Li, and A. C. Kot, "Multi-domain adversarial feature generalization for person re-identification," *arXiv preprint arXiv:2011.12563*, 2020.
- [31] Y. Ganin and V. Lempitsky, "Unsupervised domain adaptation by back-propagation," in *International conference on machine learning*. PMLR, 2015, pp. 1180–1189.
- [32] P. Chen, P. Dai, J. Liu, F. Zheng, Q. Tian, and R. Ji, "Dual distribution alignment network for generalizable person re-identification," *Thirty-Fifth AAAI Conference on Artificial Intelligence*, 2021.
- [33] Y. Yuan, W. Chen, T. Chen, Y. Yang, Z. Ren, Z. Wang, and G. Hua, "Calibrated domain-invariant learning for highly generalizable large scale re-identification," in *Proceedings of the IEEE/CVF Winter Conference on Applications of Computer Vision*, 2020, pp. 3589–3598.
- [34] I. Gulrajani and D. Lopez-Paz, "In search of lost domain generalization," *arXiv preprint arXiv:2007.01434*, 2020.
- [35] H. Zhang, Y.-F. Zhang, W. Liu, A. Weller, B. Schölkopf, and E. P. Xing, "Towards principled disentanglement for domain generalization," in *Proceedings of the IEEE/CVF Conference on Computer Vision and Pattern Recognition*, 2022, pp. 8024–8034.
- [36] Y.-F. Zhang, H. Zhang, J. Wang, Z. Zhang, B. Yu, L. Wang, D. Tao, and X. Xie, "Domain-specific risk minimization," *arXiv preprint arXiv:2208.08661*, 2022.
- [37] Y. Zhang, F. Li, Z. Zhang, L. Wang, D. Tao, and T. Tan, "Generalizable person re-identification without demographics," 2022. [Online]. Available: <https://openreview.net/forum?id=VNdFPD5wqjh>
- [38] M. Arjovsky, L. Bottou, I. Gulrajani, and D. Lopez-Paz, "Invariant risk minimization," 2020.
- [39] E. Rosenfeld, P. Ravikumar, and A. Risteski, "The risks of invariant risk minimization," 2020.
- [40] B. Schölkopf, F. Locatello, S. Bauer, N. R. Ke, N. Kalchbrenner, A. Goyal, and Y. Bengio, "Towards causal representation learning," *arXiv preprint arXiv:2102.11107*, 2021.
- [41] Y. Atzmon, F. Kreuk, U. Shalit, and G. Chechik, "A causal view of compositional zero-shot recognition," *Advances in Neural Information Processing Systems (NeurIPS)*, vol. 33, 2020.
- [42] S. Magliacane, T. van Ommen, T. Claassen, S. Bongers, P. Versteeg, and J. M. Mooij, "Domain adaptation by using causal inference to predict invariant conditional distributions," in *Advances in Neural Information Processing Systems (NeurIPS)*, 2018, pp. 10 846–10 856.
- [43] Y.-F. Zhang, H. Zhang, Z. C. Lipton, L. E. Li, and E. P. Xing, "Exploring transformer backbones for heterogeneous treatment effect estimation," *arXiv preprint arXiv:2202.01336*, 2022.
- [44] M. Besserve, A. Mehrjou, R. Sun, and B. Schölkopf, "Counterfactuals uncover the modular structure of deep generative models," in *International Conference on Learning Representations (ICLR)*, 2019.
- [45] G. Parascandolo, N. Kilbertus, M. Rojas-Carulla, and B. Schölkopf, "Learning independent causal mechanisms," in *ICML*, 2018.

- [46] T. Wang, J. Huang, H. Zhang, and Q. Sun, “Visual commonsense r-cnn,” in *Proceedings of the IEEE/CVF Conference on Computer Vision and Pattern Recognition*, 2020, pp. 10760–10770.
- [47] X. Yang, H. Zhang, and J. Cai, “Deconfounded image captioning: A causal retrospect,” *IEEE Transactions of Pattern Analysis and Machine Intelligence*, 2020.
- [48] K. Tang, J. Huang, and H. Zhang, “Long-tailed classification by keeping the good and removing the bad momentum causal effect,” in *NeurIPS*, 2020.
- [49] Z. Dong, Z. Hanwang, T. Jinhui, H. Xiansheng, and S. Qianru, “Causal intervention for weakly supervised semantic segmentation,” in *NeurIPS*, 2020.
- [50] Z. Yue, H. Zhang, Q. Sun, and X.-S. Hua, “Interventional few-shot learning,” in *NeurIPS*, 2020.
- [51] J. Pearl *et al.*, “Models, reasoning and inference,” *Cambridge, UK: Cambridge University Press*, 2000.
- [52] R. Cai, Z. Li, P. Wei, J. Qiao, K. Zhang, and Z. Hao, “Learning disentangled semantic representation for domain adaptation,” in *IJCAI: proceedings of the conference*, vol. 2019. NIH Public Access, 2019, p. 2060.
- [53] X. Sun, B. Wu, C. Liu, X. Zheng, W. Chen, T. Qin, and T.-y. Liu, “Latent causal invariant model,” *arXiv preprint arXiv:2011.02203*, 2020.
- [54] M. Hirzer, C. Beleznai, P. M. Roth, and H. Bischof, “Person re-identification by descriptive and discriminative classification,” in *Scandinavian conference on Image analysis*. Springer, 2011, pp. 91–102.
- [55] J. Pearl, M. Glymour, and N. P. Jewell, *Causal inference in statistics: A primer*. John Wiley & Sons, 2016.
- [56] R. Müller, S. Kornblith, and G. E. Hinton, “When does label smoothing help?” in *Advances in Neural Information Processing Systems*, 2019, pp. 4694–4703.
- [57] H. Zhang, M. Cisse, Y. N. Dauphin, and D. Lopez-Paz, “mixup: Beyond empirical risk minimization,” in *International Conference on Learning Representations (ICLR)*, 2018.
- [58] M. Ye, J. Shen, X. Zhang, P. C. Yuen, and S.-F. Chang, “Augmentation invariant and instance spreading feature for softmax embedding,” *IEEE transactions on pattern analysis and machine intelligence*, 2020.
- [59] W.-G. Chang, T. You, S. Seo, S. Kwak, and B. Han, “Domain-specific batch normalization for unsupervised domain adaptation,” in *Proceedings of the IEEE/CVF conference on Computer Vision and Pattern Recognition*, 2019, pp. 7354–7362.
- [60] W. Li and X. Wang, “Locally aligned feature transforms across views,” in *Proceedings of the IEEE Conference on Computer Vision and Pattern Recognition (CVPR)*, June 2013.
- [61] W. Li, R. Zhao, T. Xiao, and X. Wang, “Deepreid: Deep filter pairing neural network for person re-identification,” in *Proceedings of the IEEE Conference on Computer Vision and Pattern Recognition (CVPR)*, June 2014.
- [62] Z. Zheng, L. Zheng, and Y. Yang, “Unlabeled samples generated by gan improve the person re-identification baseline in vitro,” in *Proceedings of the IEEE International Conference on Computer Vision (ICCV)*, Oct 2017.
- [63] T. Xiao, S. Li, B. Wang, L. Lin, and X. Wang, “End-to-end deep learning for person search,” *arXiv preprint arXiv:1604.01850*, vol. 2, no. 2, 2016.
- [64] D. Gray, S. Brennan, and H. Tao, “Evaluating Appearance Models for Recognition, Reacquisition, and Tracking,” *Proc. IEEE International Workshop on Performance Evaluation for Tracking and Surveillance (PETS)*, 2007.
- [65] Z. Wei-Shi, G. Shaogang, and X. Tao, “Associating groups of people,” in *Proceedings of the British Machine Vision Conference*, 2009, pp. 23–1.
- [66] M. Sandler, A. Howard, M. Zhu, A. Zhmoginov, and L.-C. Chen, “Mobilenetv2: Inverted residuals and linear bottlenecks,” in *Proceedings of the IEEE conference on computer vision and pattern recognition*, 2018, pp. 4510–4520.
- [67] S. Lin, H. Li, C. T. Li, and A. C. Kot, “Multi-task mid-level feature alignment network for unsupervised cross-dataset person re-identification,” in *29th British Machine Vision Conference, BMVC 2018*, 2018.
- [68] S.-Z. Chen, C.-C. Guo, and J.-H. Lai, “Deep ranking for person re-identification via joint representation learning,” *IEEE Transactions on Image Processing*, vol. 25, no. 5, pp. 2353–2367, 2016.
- [69] L. Zhang, T. Xiang, and S. Gong, “Learning a discriminative null space for person re-identification,” in *Proceedings of the IEEE Conference on Computer Vision and Pattern Recognition (CVPR)*, June 2016.
- [70] W. Chen, X. Chen, J. Zhang, and K. Huang, “A multi-task deep network for person re-identification,” in *Proceedings of the Thirty-First AAAI Conference on Artificial Intelligence*, 2017, pp. 3988–3994.
- [71] S. Bai, X. Bai, and Q. Tian, “Scalable person re-identification on supervised smoothed manifold,” in *Proceedings of the IEEE Conference on Computer Vision and Pattern Recognition (CVPR)*, July 2017.
- [72] H. Zhao, M. Tian, S. Sun, J. Shao, J. Yan, S. Yi, X. Wang, and X. Tang, “Spindle net: Person re-identification with human body region guided feature decomposition and fusion,” in *Proceedings of the IEEE Conference on Computer Vision and Pattern Recognition (CVPR)*, July 2017.
- [73] M. Tamura and T. Murakami, “Augmented hard example mining for generalizable person re-identification,” *arXiv preprint arXiv:1910.05280*, 2019.
- [74] X. Pan, P. Luo, J. Shi, and X. Tang, “Two at once: Enhancing learning and generalization capacities via ibn-net,” in *Proceedings of the European Conference on Computer Vision (ECCV)*, 2018, pp. 464–479.
- [75] K. Zhou, Y. Yang, A. Cavallaro, and T. Xiang, “Learning generalisable omni-scale representations for person re-identification,” *IEEE Transactions on Pattern Analysis and Machine Intelligence*, 2021.
- [76] S. Shankar, V. Piratla, S. Chakrabarti, S. Chaudhuri, P. Jyothei, and S. Sarawagi, “Generalizing across domains via cross-gradient training,” *arXiv preprint arXiv:1804.10745*, 2018.
- [77] S. Liao and L. Shao, “Interpretable and generalizable person re-identification with query-adaptive convolution and temporal lifting,” *arXiv preprint arXiv:1904.10424*, 2019.
- [78] K. Zhou, Y. Yang, T. Hospedales, and T. Xiang, “Learning to generate novel domains for domain generalization,” in *European Conference on Computer Vision*. Springer, 2020, pp. 561–578.
- [79] S. Sagawa, P. W. Koh, T. B. Hashimoto, and P. Liang, “Distributionally robust neural networks for group shifts: On the importance of regularization for worst-case generalization,” *arXiv preprint arXiv:1911.08731*, 2019.
- [80] M. Ghifary, W. B. Kleijn, M. Zhang, and D. Balduzzi, “Domain generalization for object recognition with multi-task autoencoders,” in *Proceedings of the IEEE International Conference on Computer Vision (ICCV)*, December 2015.
- [81] M. I. Belghazi, A. Baratin, S. Rajeswar, S. Ozair, Y. Bengio, A. Courville, and R. D. Hjelm, “Mine: mutual information neural estimation,” *arXiv preprint arXiv:1801.04062*, 2018.
- [82] S. Nowozin, B. Cseke, and R. Tomioka, “f-gan: Training generative neural samplers using variational divergence minimization,” *arXiv preprint arXiv:1606.00709*, 2016.
- [83] J. Pearl, “Causal diagrams for empirical research,” *Biometrika*, vol. 82, no. 4, pp. 669–688, 1995.



Yi-Fan Zhang received the B.S. degree from south china university of technology, in 2021. He is currently pursuing the Ph.D. degree with the National Laboratory of Pattern Recognition (NLPR), Institute of Automation, Chinese Academy of Sciences (CASIA), Beijing, China. Her research interests include machine learning, and deep learning



Zhang Zhang received the B.S. degree in computer science and technology from Hebei University of Technology, Tianjin, China, in 2002, and the Ph.D. degree in pattern recognition and intelligent systems from the National Laboratory of Pattern Recognition, Institute of Automation, Chinese Academy of Sciences, Beijing, China in 2009. Currently, he is an associate professor at the National Laboratory of Pattern Recognition, Institute of Automation, Chinese Academy of Sciences (CASIA). His research interests include action and activity recognition, human attribute recognition, person re-identification, and large-scale person

retrieval. He has published 40s research papers on computer vision and pattern recognition, including some highly ranked journals and conferences, e.g., IEEE TPAMI, IEEE TIP, CVPR, and ECCV.



Da Li Da Li received the M.Eng. degree in electronics and communication engineering from Suzhou Institute of Nano-Tech and Nano-Bionics, Chinese Academy of Sciences, China, in 2013, and the Ph.D. degree in computer applications technology from the School of Artificial Intelligence, University of Chinese Academy of Sciences, China, in 2020. He is currently a Postdoc with the Center for Research on Intelligent Perception and Computing (CRIPAC), Institute of Automation, Chinese Academy of Sciences. His research interests include big visual data

and video surveillance.



Zhen Jia received his B.Eng. degree in electronic engineering from Yunnan University, Kunming, China, in 2013, and the Ph.D. degree in pattern recognition and intelligent systems from the Center for Research on Intelligent Perception and Computing, Institute of Automation, Chinese Academy of Sciences, Beijing, China, in 2020. Currently, he is a postdoctoral researcher at the Center for Research on Intelligent Perception and Computing, Institute of Automation, Chinese Academy of Sciences. His research interests include zero-shot learning, few-shot learning, and generative models.

shot learning, and generative models.



Liang Wang (Fellow, IEEE) received the B.Eng. and M.Eng. degrees from Anhui University in 1997 and 2000, respectively, and the Ph.D. degree from the Institute of Automation, Chinese Academy of Sciences (CASIA) in 2004. From 2004 to 2010, he was a Research Assistant with Imperial College London, U.K., and University, Australia, a Research Fellow with the University of Melbourne, Australia, and a Lecturer with the University of Bath, U.K., respectively. He is currently a Full Professor of the Hundred Talents Program with the National Laboratory of Pattern Recognition, CASIA. His major research interests include machine learning, pattern recognition, and computer vision. He is an IAPR Fellow

laboratory of Pattern Recognition, CASIA. His major research interests include machine learning, pattern recognition, and computer vision. He is an IAPR Fellow



Tieniu Tan (Fellow, IEEE) received the B.Sc. degree in electronic engineering from Xi'an Jiaotong University, China, in 1984, and the M.Sc. and Ph.D. degrees in electronic engineering from Imperial College London, U.K., in 1986 and 1989, respectively. He is currently a Professor with Center for Research on Intelligent Perception and Computing, NLPR, CASIA, China. He has published more than 450 research papers in refereed international journals and conferences in the areas of image processing, computer vision, and pattern recognition,

and has authored or edited 11 books. His research interests include biometrics, image and video understanding, information hiding, and information forensics. He is a Fellow of CAS, TWAS, BAS, IAPR, and the U.K. Royal Academy of Engineering, and the Past President of IEEE Biometrics Council